Equation of state with an extended SU(3) quark-meson model under conditions prevailing in core collapse supernovae

Thomas Beisitzer,[1,*] Rainer Stiele,[1,†] and Jürgen Schaffner-Bielich[1,2,3,‡]

[1]*Institut für Theoretische Physik, Universität Heidelberg, Philosophenweg 16, D-69120 Heidelberg, Germany*

[2]*Institut für Theoretische Physik, Goethe-Universität Frankfurt, Max-von-Laue-Straße 1, D-60438 Frankfurt am Main, Germany*

[3]*ExtreMe Matter Institute EMMI, GSI Helmholtzzentrum für Schwerionenforschung GmbH, Planckstraße 1, D-64291 Darmstadt, Germany*

(Received 8 April 2014; published 2 October 2014)

The quark-meson model is investigated for the two- and three-flavor case extended by contributions of vector mesons under conditions encountered in core-collapse supernova matter. Typical temperature ranges, densities, and electron fractions, as found in core-collapse supernova simulations, are studied by implementing charge neutrality and local β equilibrium with respect to weak interactions. Within this framework, we analyze the resulting phase diagram and equation of state (EoS) and investigate the impact of undetermined parameters of the model. The EoS turns out to be relatively independent on the entropy per baryon but there are significant changes when going from the two-flavor to the three-flavor case due to the nontrivial contribution from the strange quarks which stay massive even at high densities. While an increasing vector meson coupling constant leads to a substantial stiffening of the EoS, we find that the impact of changing the scalar meson mass is equally strong and results in a softening of the EoS for increasing values.

DOI: 10.1103/PhysRevD.90.085001 PACS numbers: 12.38.Mh, 12.39.Ba, 97.60.Bw

I. INTRODUCTION

The properties of strong interaction matter as described by quantum chromodynamics (QCD) at high densities and temperatures can be studied in the laboratory by relativistic heavy-ion collision experiments. Manifestations of this extreme state of matter created in the laboratory can be found in the early universe, neutron star mergers, and core-collapse supernova explosions.

The processes which are able to turn the collapse of a massive star into a supernova explosion are not fully understood yet; see e.g. [1] for a review. A key ingredient to core-collapse supernova simulations is the nuclear equation of state at nonzero density, temperature, and proton fraction. During the supernova evolution high temperatures and densities can be reached allowing for the opportunity to explore unknown regimes of the phase diagram of strong interactions, i.e. the QCD phase diagram. The conditions might be such that a new phase emerges in the core of the collapsed star.

A possible phase transition during the supernova evolution has been studied in [2] for a pion-condensed state and in [3,4] for a first-order phase transition from hadronic matter to quark matter which can influence the supernova dynamics such that a delayed explosion can take place. Quark matter could also appear during the later protoneutron star evolution as studied in [5]. The presence of a new quark matter phase during the supernova stage has been studied in more detail in [6,7] by including effects from neutrinos. If a new phase is present early in the evolution of the supernova, it can produce a second shock wave with an accompanying measurable second neutrino burst [8]. In certain cases, different paths in the phase diagram of QCD can be swept out by the delayed collapse to a black hole during the evolution of a core-collapse supernova [9]. The adopted equations of state (EoS) used above are hybrid models with a low-density nucleonic equation of state and the simple MIT bag model extended to nonzero temperatures as the high-density part. The merger of pure quark stars (strange stars) was also simulated within the MIT bag model in [10] showing distinctly different features compared to ordinary neutron star mergers [11].

However, it is known that the MIT bag model fails in describing lattice data, see e.g. [12], and is not suited to describe profound features of dense matter QCD, as chiral symmetry restoration at high densities. As perturbation theory breaks down on the scale of interest here and results from lattice QCD at high densities are not available yet, improved effective models have to be utilized for studying the regime of the QCD plasma relevant for astrophysical applications, as core-collapse supernovae, which we focus on in the following. The Nambu-Jona-Lasinio (NJL) model, as a chiral effective model of QCD, has been studied for nonzero temperature and neutrino chemical

*beisitzer@thphys.uni-heidelberg.de
†r.stiele@thphys.uni-heidelberg.de
‡schaffner@astro.uni-frankfurt.de

potential, relevant for protoneutron stars, in [13–16]. First exploratory investigations of supernova explosions, which require a given electron to baryon number ratio Y_e, were only undertaken recently within chiral approaches of QCD in [17]. Here the Polyakov-loop extended version of the NJL model, the PNJL model, was used and compared to the MIT bag model. It turned out that there are generic differences between the two model descriptions of relevance for the supernova dynamics.

In this work the linear sigma model [18] is adopted as an effective chiral model of QCD to study the high-density plasma phase, where the fundamental particles are quarks interacting via scalar and vector meson exchange. The quark masses are generated by nonvanishing vacuum expectation values of the scalar fields which act as chiral condensates and model the spontaneous breaking of chiral symmetry as observed in the vacuum of QCD. At high temperature and/or densities the condensates melt away and the theory becomes approximately chirally invariant. The order of the phase transition depends on the choice of the parameters used. A detailed study is performed by varying the different parameters of the model to delineate their role for the properties of supernova material. A comparison between the two flavor model, involving only the light up and down quarks, and the three flavor model, where also the strange quark is taken into account, is performed. By using standard methods of finite temperature field theory, the EoS is calculated as an improved description of the high-density QCD plasma phase compared to the MIT bag model result. Matching the EoS to a hadronic EoS unless quark matter is absolutely stable can serve as an input for core-collapse supernova and neutron star merger simulations.

II. EXTENDED LINEAR SIGMA MODEL

A. Standard quark-meson model

The Lagrangian of the linear sigma model with N_f flavors is given by (see e.g. [19])

$$\mathcal{L} = \bar{\psi}(i\partial - g\phi)\psi + \mathcal{L}_{N_f}, \tag{1}$$

$$\phi = T_a\phi_a = T_a(\sigma_a + i\gamma_5\pi_a). \tag{2}$$

The quark spinors are of the form $\psi = (u, d)$ for $N_f = 2$ flavors and $\psi = (u, d, s)$ for $N_f = 3$ and involve also the color degrees of freedom $N_c = 3$. The Yukawa coupling between quarks and members of the scalar or pseudoscalar meson nonets σ_a/π_a is controlled by the scalar coupling constant g. The generators of the underlying $U(N_f)$ symmetry group are denoted by $T_a = \lambda_a/2$ with $a = 0, \ldots, N_f^2 - 1$, which are the Pauli matrices or the Gell-Mann matrices. The pure mesonic contributions $\mathcal{L}_{N_f}$ for N_f flavors are of the form [18,20]

$$\mathcal{L}_2 = \frac{1}{2}\partial_\mu\sigma\partial^\mu\sigma + \frac{1}{2}\partial_\mu\vec{\pi}\partial^\mu\vec{\pi} - \frac{\lambda}{4}((\vec{\pi}^2 + \sigma^2) - v^2)^2 + h\sigma, \tag{3}$$

$$\mathcal{L}_3 = \mathrm{Tr}(\partial_\mu\phi^\dagger\partial^\mu\phi) - m^2\mathrm{Tr}(\phi^\dagger\phi) - \lambda_1[\mathrm{Tr}(\phi^\dagger\phi)]^2 - \lambda_2\mathrm{Tr}(\phi^\dagger\phi)^2 + c(\det(\phi) + \det(\phi^\dagger)) + \mathrm{Tr}[H(\phi + \phi^\dagger)]. \tag{4}$$

The first part of Eq. (3) is the standard kinetic term for the mesons, while the potential part involves the Mexican hat potential, which is invariant under chiral transformations and leads to spontaneous symmetry breaking, as well as an explicit symmetry breaking term, controlled by the parameter h. These symmetry breaking terms generate a finite vacuum expectation value (VEV) for the σ meson and thus a finite quark mass through (1).

The parameter v is determined by the requirement that the minimum of the potential lies at the pion decay constant f_π and the fact that the VEV of the pion field has to vanish due to its parity. From this follows

$$v^2 = f_\pi^2 - \frac{h}{\lambda f_\pi}. \tag{5}$$

The masses of the π and σ mesons in the ground state are given by the second derivatives of the potential with respect to the fields evaluated in the vacuum at $T = 0$ which fixes

$$h = f_\pi m_\pi^2, \tag{6}$$

$$\lambda = \frac{m_\sigma^2 - m_\pi^2}{2f_\pi^2}. \tag{7}$$

The pion mass is directly related to the explicit symmetry breaking term and for $h = 0$ the pions become the massless Goldstone bosons. The light quark masses are given according to

$$m_l = \frac{g}{2}\langle\sigma\rangle. \tag{8}$$

The Lagrangian (4) for three flavors contains also a standard kinetic term, as well as a meson mass term. Additionally, there are quartic interaction terms involving the coupling constants λ_1 and λ_2. The determinant term is a cubic coupling term between the fields, which corresponds to the $U(1)_A$ anomaly. The last part is again an explicit symmetry breaking term, with $H = h_a T_a$. Analogously to the $SU(2)$ case, through the spontaneous symmetry breaking, the σ fields get nonvanishing VEVs, while again the VEVs of the π fields have to vanish due to their pseudoscalar character. Following [20] we introduce the notation

$$\langle\phi\rangle \equiv \bar{\phi} \equiv T_a\bar{\sigma}_a. \tag{9}$$

Shifting ϕ by their VEVs and taking into account that only $\bar{\sigma}_0$, $\bar{\sigma}_3$, and $\bar{\sigma}_8$ do not vanish, because they respect the quantum numbers of the vacuum, the potential takes the form [21]

$$\begin{aligned} U(\bar{\sigma}_0,\bar{\sigma}_3,\bar{\sigma}_8) = {} & m^2\left(\frac{\bar{\sigma}_0^2+\bar{\sigma}_3^2+\bar{\sigma}_8^2}{2}\right) - c\left(\frac{\bar{\sigma}_0^3}{3\sqrt{6}} - \frac{\bar{\sigma}_8^3}{6\sqrt{3}} - \frac{\bar{\sigma}_0\bar{\sigma}_3^2}{2\sqrt{6}} - \frac{\bar{\sigma}_0\bar{\sigma}_8^2}{2\sqrt{6}} + \frac{\bar{\sigma}_3^2\bar{\sigma}_8}{2\sqrt{3}}\right) \\ & + \lambda_1\left(\frac{\bar{\sigma}_0^4+\bar{\sigma}_3^4+\bar{\sigma}_8^4}{4} + \frac{\bar{\sigma}_0^2\bar{\sigma}_3^2+\bar{\sigma}_0^2\bar{\sigma}_8^2+\bar{\sigma}_3^2\bar{\sigma}_8^2}{2}\right) \\ & + \lambda_2\left(\frac{\bar{\sigma}_0^4}{12} + \frac{\bar{\sigma}_3^4+\bar{\sigma}_8^4}{8} + \frac{\bar{\sigma}_0^2\bar{\sigma}_3^2+\bar{\sigma}_0^2\bar{\sigma}_8^2}{2} + \frac{\bar{\sigma}_3^2\bar{\sigma}_8^2}{4} + \frac{\bar{\sigma}_0\bar{\sigma}_3^2\bar{\sigma}_8}{\sqrt{2}} - \frac{\bar{\sigma}_0\bar{\sigma}_8^3}{3\sqrt{2}}\right) - h_0\bar{\sigma}_0 - h_3\bar{\sigma}_3 - h_8\bar{\sigma}_8. \end{aligned} \tag{10}$$

The σ fields are identified with the known scalar mesons and the π fields with the pseudoscalar ones

$$(\sigma_0,\ldots,\sigma_8)^{\mathrm{T}} \mathrel{\hat{=}} (\sigma_0, a_0^+, a_0^-, \sigma_3, \kappa^+, \kappa^-, \kappa^0, \bar{\kappa}^0, \sigma_8)^{\mathrm{T}}, \tag{11}$$

$$(\pi_0,\ldots,\pi_8)^{\mathrm{T}} \mathrel{\hat{=}} (\pi_0, \pi^+, \pi^-, \pi_3, K^+, K^-, K^0, \bar{K}^0, \pi_8)^{\mathrm{T}}. \tag{12}$$

Their masses can be computed analogously to the $SU(2)$ case from the potential part of the Lagrangian (4) through [20]

$$(m_S^2)_{ab} = \left.\frac{\partial^2 U(\sigma,\pi)}{\partial\sigma_a\partial\sigma_b}\right|_{\bar{\sigma}}, \tag{13}$$

$$(m_P^2)_{ab} = \left.\frac{\partial^2 U(\sigma,\pi)}{\partial\pi_a\partial\pi_b}\right|_{\bar{\sigma}}. \tag{14}$$

The condensate σ_3 breaks isospin symmetry explicitly. It is assumed that the vacuum at zero temperature is isospin symmetric, so that there holds $\sigma_3 = 0$. Thus, the explicit symmetry breaking term has to vanish, $h_3 = 0$. The quark masses are given by

$$\begin{aligned} m_u &= g\left(\frac{1}{\sqrt{6}}\bar{\sigma}_0 + \frac{1}{2}\bar{\sigma}_3 + \frac{1}{2\sqrt{3}}\bar{\sigma}_8\right), \\ m_d &= g\left(\frac{1}{\sqrt{6}}\bar{\sigma}_0 - \frac{1}{2}\bar{\sigma}_3 + \frac{1}{2\sqrt{3}}\bar{\sigma}_8\right), \\ m_s &= g\left(\frac{1}{\sqrt{6}}\bar{\sigma}_0 - \frac{1}{\sqrt{3}}\bar{\sigma}_8\right). \end{aligned} \tag{15}$$

The remaining parameters can then be determined as in Refs. [19,20].

B. Extension to vector mesons

The standard linear sigma model is extended by a vector meson contribution. The interaction of quarks through scalar mesons is attractive while a repulsive force can be provided by the inclusion of vector mesons. The Lagrangian of the vector mesons is given by [22]

$$\mathcal{L}_V = -\frac{1}{4}F^{\mu\nu}F_{\mu\nu} + \frac{\eta_v^2}{2}V^{a\mu}V_\mu^a - g_V^a\bar{\psi}\gamma^\mu T^a\psi V_\mu^a, \tag{16}$$

where V_μ^a are the vector meson fields. Their number depends on the considered flavors, which are

$$a = 0,\ldots,3 \quad \text{for } SU(2), \tag{17}$$

$$a = 0,\ldots,8 \quad \text{for } SU(3). \tag{18}$$

The T^a are again the generators of the appropriate groups. The Lorentz index μ indicates the vector character of the mesons. The first term in Eq. (16) is the standard kinetic term for vector particles, while the second one is the mass term. The vector mesons are coupled to the quark fields by a Yukawa type interaction term.

C. Grand canonical potential

Assuming local equilibrium allows one to work in a mean field approximation. The meson fields are treated as classical fields. As pointed out before, the VEVs of the pion fields have to vanish due to parity while the σ fields adopt a finite value. In the case of three flavors a finite VEV is only investigated for the σ_0, σ_3, and σ_8 fields and it is assumed for the others to vanish. Furthermore, the spatial components of the vector meson fields have to vanish because of rotational symmetry. Additionally, for two flavors only the zeroth and third flavor group component do not vanish because of isospin invariance. For three flavors one ends up with an additional vector meson field from the eighth component of the vector field nonet. The mathematical vector fields can be directly identified with the physical ones. For $N_f = 2$ one finds

$$\omega \mathrel{\hat{=}} \bar{V}_0^0, \qquad \rho \mathrel{\hat{=}} \bar{V}_0^3. \tag{19}$$

For $N_f = 3$ one decouples the strange quark sector by assuming ideal mixing and one finds

$$\omega \widehat{=} \sqrt{\frac{2}{3}}\bar{V}_0^0 + \frac{1}{\sqrt{3}}\bar{V}_0^8, \qquad \rho \widehat{=} \bar{V}_0^3,$$
$$\phi \widehat{=} \frac{1}{\sqrt{3}}\bar{V}_0^0 - \sqrt{\frac{2}{3}}\bar{V}_0^8. \tag{20}$$

The rotation of fields into each other results in the change of the effective coupling constants according to

$$\frac{g_V}{2} = g_\omega = g_\rho = \frac{g_\phi}{\sqrt{2}} \tag{21}$$

as dictated by $SU(3)$ symmetry and ideal mixing. The fields occur in combination with the Gell-Mann matrices, that is why also the physical fields have to be given with respect to a basis which is defined as

$$\chi^\omega = \begin{pmatrix} 1 & 0 & 0 \\ 0 & 1 & 0 \\ 0 & 0 & 0 \end{pmatrix} \qquad \chi^\rho = \begin{pmatrix} 1 & 0 & 0 \\ 0 & -1 & 0 \\ 0 & 0 & 0 \end{pmatrix}$$
$$\chi^\phi = \begin{pmatrix} 0 & 0 & 0 \\ 0 & 0 & 0 \\ 0 & 0 & 1 \end{pmatrix}. \tag{22}$$

The $SU(2)$ mean field Lagrangian is then given by

$$\mathcal{L} = \bar{\psi}\left(i\partial\!\!\!/ + \mu\gamma^0 - \frac{g}{2}\sigma - g_\omega\gamma^0\omega - g_\rho\gamma^0\tau^3\rho\right)\psi \tag{23}$$

$$-\frac{\lambda}{4}(\sigma^2 - v^2)^2 + h\sigma + \frac{m_\omega^2}{2}\omega^2 + \frac{m_\rho^2}{2}\rho^2. \tag{24}$$

Here also the chemical potential was added. It is a diagonal matrix with the entries μ_u and μ_d. The vector meson contributions are of the same form and one defines an effective chemical potential

$$\tilde{\mu} = \begin{pmatrix} \tilde{\mu}_u & 0 \\ 0 & \tilde{\mu}_d \end{pmatrix} = \begin{pmatrix} \mu_u - g_\omega\omega - g_\rho\rho & 0 \\ 0 & \mu_d - g_\omega\omega + g_\rho\rho \end{pmatrix}. \tag{25}$$

Now we turn to the case of SU(3) flavor symmetry. Analog to the vector meson fields, also the condensates are rotated to decouple the strange and nonstrange sectors [19,20]

$$\begin{pmatrix} \sigma_x \\ \sigma_y \end{pmatrix} = \frac{1}{\sqrt{3}}\begin{pmatrix} \sqrt{2} & 1 \\ 1 & -\sqrt{2} \end{pmatrix}\begin{pmatrix} \sigma_0 \\ \sigma_8 \end{pmatrix}, \tag{26}$$

where σ_x is called the nonstrange condensate and σ_y the strange condensate. Using this new notation the meson potential is rewritten and the $SU(3)$ mean field Lagrangian takes the form

$$\mathcal{L} = \bar{\psi}\left[i\partial\!\!\!/ + \mu\gamma^0 - g\left(\sigma_0\frac{\lambda^0}{2} + \sigma_3\frac{\lambda^3}{2} + \sigma_8\frac{\lambda^8}{2}\right) - g_\omega\gamma^0\omega\chi^\omega - g_\rho\gamma^0\rho\chi^\rho - g_\phi\gamma^0\phi\chi^\phi\right]\psi$$
$$- \frac{m^2}{2}(\sigma_x^2 + \sigma_y^2 + \sigma_3^2) + \frac{c}{2\sqrt{2}}(\sigma_x^2\sigma_y - \sigma_3^2\sigma_y) - \frac{1}{8}(2\lambda_1 + \lambda_2)(\sigma_x^4 + \sigma_3^4) - \frac{1}{4}(\lambda_1 + \lambda_2)\sigma_y^4$$
$$- \frac{\lambda_1}{2}(\sigma_x^2\sigma_y^2 + \sigma_3^2\sigma_y^2 + \sigma_x^2\sigma_3^2) - \frac{3}{4}\lambda_2\sigma_x^2\sigma_3^2 + h_x\sigma_x + h_y\sigma_y + \frac{m_\omega^2}{2}\omega^2 + \frac{m_\rho^2}{2}\rho^2 + \frac{m_\phi^2}{2}\phi^2. \tag{27}$$

The chemical potential gets an additional entry for the strange quark of the form $\tilde{\mu}_s = \mu_s - g_\phi\phi$. The grand canonical potential is connected to the Lagrangian through the path integral over the quark fields, which are the only remaining quantum fields

$$\Omega = -\frac{T}{V}\ln\mathcal{Z}, \tag{28}$$

$$\mathcal{Z} = \int \mathcal{D}\bar{\psi}\mathcal{D}\psi \exp\left[\int_0^\beta \mathrm{d}\tau \int \mathrm{d}^3x\mathcal{L}(\bar{\psi},\psi)\right]. \tag{29}$$

with the temperature T and $\beta = 1/T$. The electron contribution is omitted here, since it is fully decoupled and can be computed straightforward. The interesting thermodynamic quantities can be derived from the grand canonical potential through the standard equations from statistical physics,

$$p = -\Omega, \qquad s = -\left.\frac{\partial\Omega}{\partial T}\right|_{\mu_i=\text{const}}, \qquad n_i = -\left.\frac{\partial\Omega}{\partial\mu_i}\right|_{T=\text{const}}, \tag{30}$$

$$\epsilon = Ts + \Omega + \sum_i \mu_i n_i. \tag{31}$$

The values of the condensates and vector meson fields are computed by solving the gap equations

$$SU(2): \quad \frac{\partial\Omega}{\partial\sigma} = \frac{\partial\Omega}{\partial\omega} = \frac{\partial\Omega}{\partial\rho} = 0, \tag{32}$$

$$SU(3): \quad \frac{\partial\Omega}{\partial\sigma_x} = \frac{\partial\Omega}{\partial\sigma_y} = \frac{\partial\Omega}{\partial\sigma_3} = \frac{\partial\Omega}{\partial\omega} = \frac{\partial\Omega}{\partial\rho} = \frac{\partial\Omega}{\partial\phi} = 0 \tag{33}$$

in the mean field approximation.

D. Parameter fixing

As described before, the parameters of the potentials are fixed by using measured meson masses and decay constants given by the Particle Data Group [23]. For the $SU(2)$ case it is used

$$\begin{aligned} m_{\pi^\pm} &= 140 \text{ MeV}, & m_{\pi^0} &= 135 \text{ MeV}, \\ m_\omega &= 783 \text{ MeV}, & m_\rho &= 775 \text{ MeV}, \end{aligned} \tag{34}$$

with $f_\pi = 92$ MeV. Since we do not distinguish between the different pions, an averaged value is used. In the $SU(3)$ case more values need to be fixed, additionally

$$\begin{aligned} m_{K^\pm} &= 494 \text{ MeV}, & m_{K^0} &= 498 \text{ MeV}, \\ m_\eta &= 548 \text{ MeV}, & m_{\eta'} &= 958 \text{ MeV}, \\ f_K &= 110 \text{ MeV}, & m_\phi &= 1019 \text{ MeV} \end{aligned} \tag{35}$$

are used, where again the kaon masses are averaged. The scalar coupling constant g is fixed by the constituent light quark mass $m_l = 300$ MeV.

To solve Eqs. (32) or (33) also the temperature and chemical potentials have to be known. They are computed by implementing constraints, corresponding to supernova matter. The baryon density is fixed and given by

$$n_B = \frac{n_u + n_d + n_s}{3}. \tag{36}$$

As further input in supernovae simulations the electron-baryon ratio Y_e is fixed according to

$$Y_e \equiv \frac{n_e}{n_B} = \frac{3n_e}{n_u + n_d + n_s}. \tag{37}$$

As a standard value $Y_e = 0.2$ is used for the typical value at core bounce of a supernova, following [17]. Demanding electric charge neutrality yields the condition

$$0 = q_u n_u + q_d n_d + q_s n_s + q_e n_e, \tag{38}$$

with the corresponding charges q_i of the quarks and the electron. Additionally, local equilibrium with respect to the weak interaction process $s + u \leftrightarrow d + u$ is assumed for three flavors, from which it follows that $\mu_d = \mu_s$.

During the supernova explosion temperatures of several tens of MeV are reached [24]. The entropy gives a constraint to determine the temperature relevant for supernova explosions. For the variation limits of the entropy we use [24] as guidance. So we choose a standard value of one k_B per baryon and explore the interval of $0.5 - 4k_B$/baryon.

Not all parameters can be fixed; the remaining ones are varied in the further analysis. The vector coupling is altered around a chosen standard value of $g_\omega = 3.0$ within an order of magnitude, since it should be in the same range as the scalar coupling g.

The mass of the σ meson is not determined well experimentally yet. Recently, it has been identified with the resonance $f_0(500)$ [23] that has replaced the broad $f_0(600)$ resonance. Other approaches assign the $f_0(1370)$ resonance with the σ meson [25]. Hence, it will be varied in the range of (400–1000) MeV, but the standard value $m_\sigma = 600$ MeV is used [19]. The upper bound is determined by the fact that the model saturates around $m_\sigma \approx 1100$ MeV [19].

To study the influence of the electron-baryon rate, Y_e will also be varied in the range (0.0–0.5).

III. PHASE DIAGRAM

In Fig. 1 the phase diagram for the $SU(2)$ and $SU(3)$ flavor case for $Y_e = 0.2$ and $Y_e = 0.5$ is shown. A first-order phase transition is observed for all cases at low temperatures represented by the solid lines. This phase transition is associated with the approximate restoration of chiral symmetry in the light quark sector where the σ_x field serves as a corresponding order parameter.

For both flavor cases a critical endpoint is observed which lies approximately at the same temperature ($T \approx 80$ MeV). For higher temperatures the phase transition is a crossover, i.e. the system goes smoothly from one phase into the other so that no jump in the order parameter appears and no mixed phase of the low- and high-density

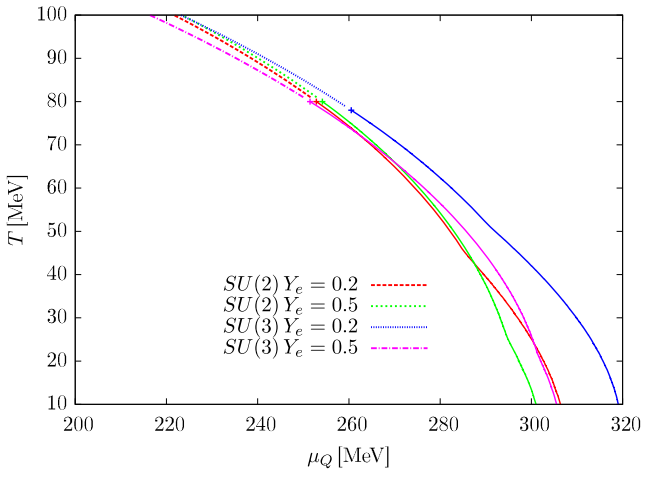

FIG. 1 (color online). Phase diagram in $\mu_Q - T$ space for the different flavor cases, with the standard Y_e values, $g_\omega = 3.0$, $m_\sigma = 600$ MeV.

phase is present. The phase transition lines for the different cases shown are quite close to each other. However, one recognizes that for a lower electron fraction the phase transition happens at lower quark chemical potential for the three flavor case. The phase transition line for $N_f = 3$ is located at higher quark chemical potential compared to $N_f = 2$ for $Y_e = 0.2$.

The location of the transition line is similar to the findings in [19] for the QM model. Small differences are present even for the isospin symmetric case and should account for the fact that effects from vector meson exchange are considered here, which are expected to be of more relevance for the high-density moderate temperature region of the QCD phase diagram of interest in the present study.

In the following the change of the transition line due to changes in the parameters will be illustrated in more detail.

To understand the phase transition structure, the evolution of the relevant scalar fields shall be discussed. We find that only the nonstrange condensate σ_x shows a strong jump across the phase transition line and reaches values close to the one of a chirally fully restored phase. Although a small jump in the strange scalar field σ_y is observed, its value stays high (over 0.5) and so the strange quarks remain massive. This behavior is expected, as electric charge neutrality and the electron fraction are implemented. Since the up quark is the only remaining positively charged particle and down and strange chemical potentials are the same, the density of the strange quark has to be suppressed by a large mass term, represented by a large value of σ_y. Following this, for lower values of Y_e the strange quark condensate melts away at lower densities, as a higher number density of strange quarks is favored.

The value of the third scalar field, σ_3, relevant for isospin breaking effects, stays always low, so that the mass difference between up and down quark remains small.

Figure 2 shows how the electron fraction influences the phase diagram for three quark flavors. The phase transition takes place at lower quark chemical potential for an increased electron fraction. For a higher value of Y_e the strange quark gets suppressed, because of charge neutrality, and so the light quark density is higher leading to a larger contribution in the gap equation and an onset of the chiral phase transition at lower densities. For the $SU(2)$ case the system is not as sensitive to changes in Y_e as for the three flavor case, since the strange quarks are not available to be replaced by the light quarks.

The dependence of the phase transition line on the vector coupling g_ω is shown in Fig. 3. The phase transition gets smoother with increasing vector coupling constant because of the repulsive character of the vector mesons. Thus, the jumps in the condensates become smaller, until the transition is a crossover at all considered temperatures. The transition line also moves to higher quark chemical potential μ_Q, since the effective chemical potentials are lowered as the vector meson contribution increases with

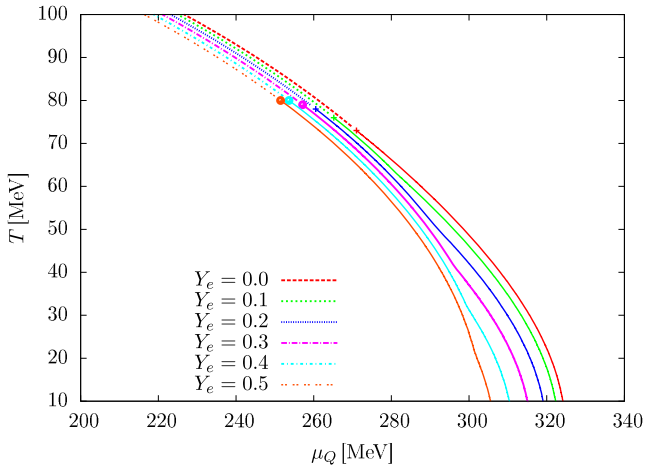

FIG. 2 (color online). $SU(3)$ phase diagram in $\mu_Q - T$ space for different Y_e with $g_\omega = 3.0$, $m_\sigma = 600$ MeV. The phase transition line is shifted to lower values of μ_Q for increasing Y_e.

increasing g_ω. Therefore a larger μ_Q is needed for the phase transition to happen. Our findings are in line with the results in the Nambu-Jona-Lasinio model with vector interactions; see e.g. Ref. [26,27].

The critical endpoint is located at lower temperature for increasing values of g_ω, as it is expected from the discussion above, but it varies only slightly between the different flavor and Y_e cases. For $g_\omega = 9.0$ the critical endpoint vanishes from the phase diagram, so that the phase transition is always a crossover. Additionally, it is observed that the sensitivity to changes in g_ω is much higher compared to the changes in Y_e.

Figure 4 illustrates the changes of the phase diagram with the mass of the σ meson m_σ. For very high σ masses

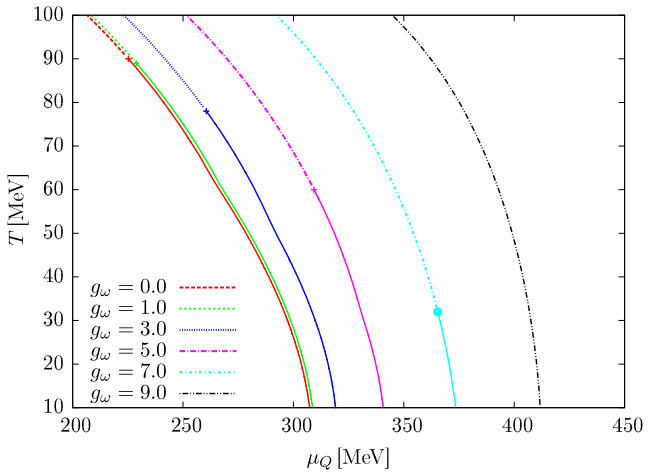

FIG. 3 (color online). $SU(3)$ phase diagram in $\mu_Q - T$ space for $Y_e = 0.2$, $m_\sigma = 600$ MeV and different vector coupling constants g_ω. The critical endpoint moves to smaller temperatures for an increase in g_ω until the phase transition is a crossover over the whole plane. The transition line moves to larger μ_Q for growing g_ω.

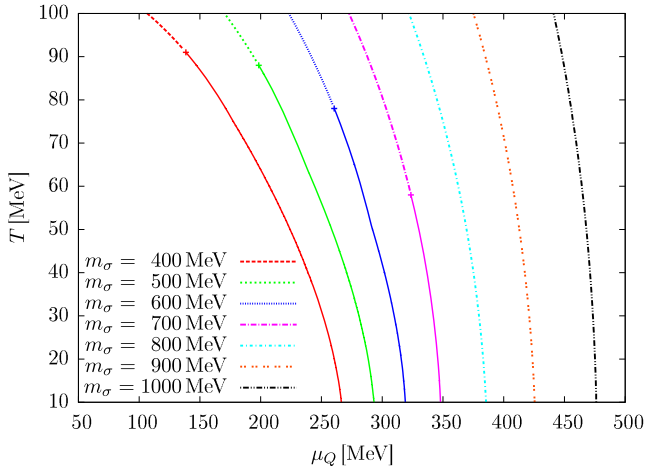

FIG. 4 (color online). $SU(3)$ phase diagram in $\mu_Q - T$ space for $Y_e = 0.2$, $g_\omega = 3.0$ and different scalar meson masses m_σ. The critical endpoint moves to lower temperatures for increasing m_σ, until for all temperatures a crossover is observed. The transition line moves to larger μ_Q for higher values of m_σ.

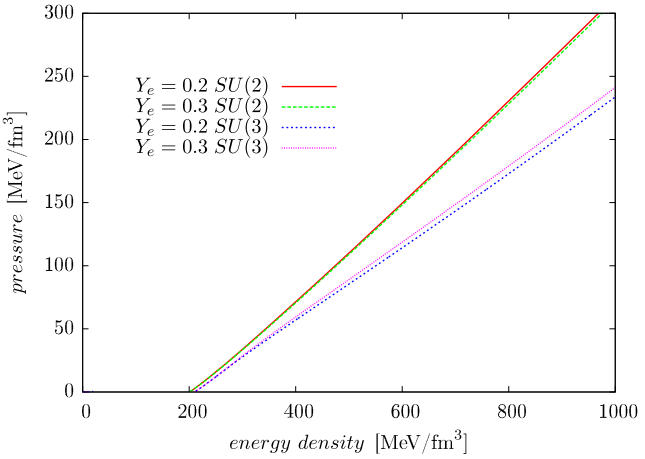

FIG. 5 (color online). Quark-meson matter equation of state for different Y_e and number of flavors with $s = 1.0k_B$/baryon, $g_\omega = 3.0$, $m_\sigma = 600$ MeV. A nearly linear relation between pressure and energy is found. At a given energy density, the two flavor case provides a larger pressure compared to the three flavor one with a larger slope. The nonzero energy density at vanishing pressure is due to the used Maxwell construction from the vacuum to the matter phase. At $T = 0$ MeV no quarks are present before the phase transition takes place.

the phase transition does not take place until very high chemical potentials are reached, as also seen in Ref. [19]. The role of m_σ can be understood more easily within the $SU(2)$ model. The σ mass fixes the λ parameter in the meson potential. Thus for an increasing m_σ also λ increases and the potential becomes deeper. Therefore, more energy is needed to develop the second minimum and the phase transition is shifted to higher values of μ_Q and becomes smoother. For the $SU(3)$ case the situation is less transparent, since the scalar meson mass is fixed by solving a system of nonlinear equations [19,20]. However, the dependence of the phase transition line on m_σ turns out to be the same. For large values of m_σ, the phase transition is always a crossover, as it was also observed for large values of the vector coupling constant g_ω, i.e. for a large vector repulsion between the quarks.

For a lower σ meson mass the phase transition appears at considerably smaller values of μ_Q. Note, that the effect of a lower value of m_σ can be compensated by an increase in the vector coupling g_ω to shift the phase transition line back to larger values of μ_Q. In the m_σ parameter range that is considered here, the changes of the critical quark chemical potential are similar to the case when the vector coupling constant g_ω is varied within the adopted range considered to be natural. But one should recall, that the g_ω parameter range was only fixed by analogy arguments, while the mass m_σ is varied according to the mass range motivated by experimental data.

IV. EQUATION OF STATE

In the following, we consider quark-meson matter under conditions prevailing in core collapse supernovae which evolves adiabatically at a fixed entropy per baryon s. We stress that the results presented here are the equation of state of the high-density QCD plasma phase. Thus they should be matched at low-energy densities to a hadronic EoS for most cases, unless strange quark matter is absolutely stable at vanishing temperature.

In Fig. 5 the equation of state is shown for a fixed value of $s = 1.0k_B$/baryon for the $SU(2)$ and $SU(3)$ flavor cases. The value of $Y_e = 0.3$ was chosen to compare our results with Ref. [17].

One notices that the quark-meson matter equation of state has a larger slope in the $SU(2)$ flavor case compared to the $SU(3)$ flavor case. The electron fraction Y_e has a very little influence on the equation of state. It seems that the computed EoS in the SU(3) case follows approximately the EoS of a free gas of relativistic massless particles, $p = \epsilon/3$, as chiral symmetry is approximately restored. However, due to the explicit symmetry breaking terms the particles are never really massless. Additionally, there is a contribution from the vector mesons. Both effects combine to the observed slope of the EoS. For two flavors the system with a smaller electron fraction has a larger pressure, while for three flavors the pressure in the system with more electrons is higher. The difference between the $SU(2)$ and $SU(3)$ flavor cases is due to the presence of the strange quark, which does not become massless [28]. The EoS for the $SU(3)$ case with a higher electron fraction lies above the one with the lower electron fraction, because the strange quark fraction is lower in the first case.

The effect of varying the entropy per baryon is shown in Fig. 6. The differences are so small that the lines lie nearly on top of each other for all values of s in the given interval.

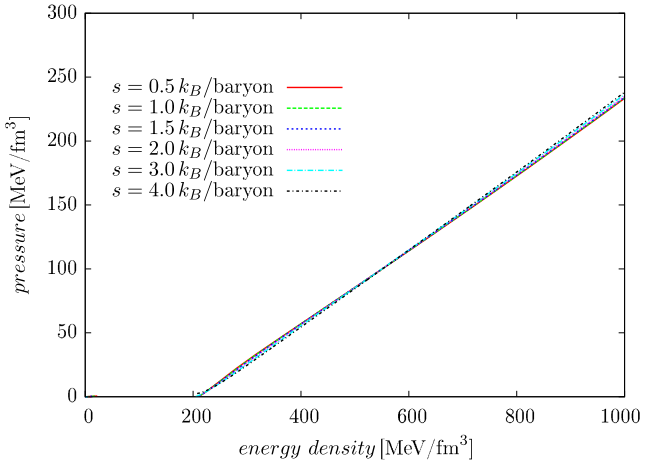

FIG. 6 (color online). $SU(3)$ quark-meson matter equation of state for $Y_e = 0.2$ and different entropy per baryon values s with $g_\omega = 3.0$, $m_\sigma = 600$ MeV. The different cases lie nearly on top of each other.

This is caused by the low temperatures involved, so that the thermal contributions are small while the shape of the quark-meson matter EoS is mostly determined by the chemical potentials and the interactions.

For an increasing value of g_ω the slopes of the quark-meson matter equations of state rise, as shown in Fig. 7. This behavior is quite generic and well known from the relativistic $\sigma - \omega$ model for nuclear matter [29,30] and is also seen in NJL model calculations with vector coupling terms; see e.g. the discussion in [31] and Ref. [32] for an explicit plot. In principal the EoS would eventually reach the limit $p = \epsilon$, which would mean that the speed of sound equals the speed of light setting the causal limit.

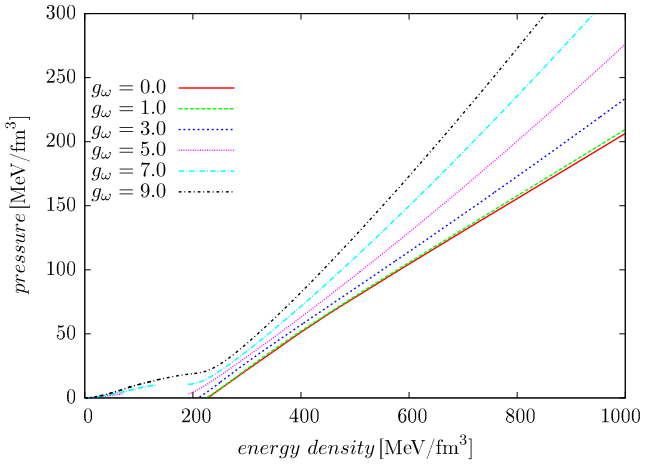

FIG. 7 (color online). $SU(3)$ quark-meson matter equation of state for $Y_e = 0.2$, $s = 1.0k_B$/baryon, $m_\sigma = 600$ MeV and different vector meson couplings g_ω. At small energy densities one recognizes that the mixed phase region of the vacuum and the matter phase gets smaller with increasing g_ω. The slope of the EoS increases for larger values of g_ω.

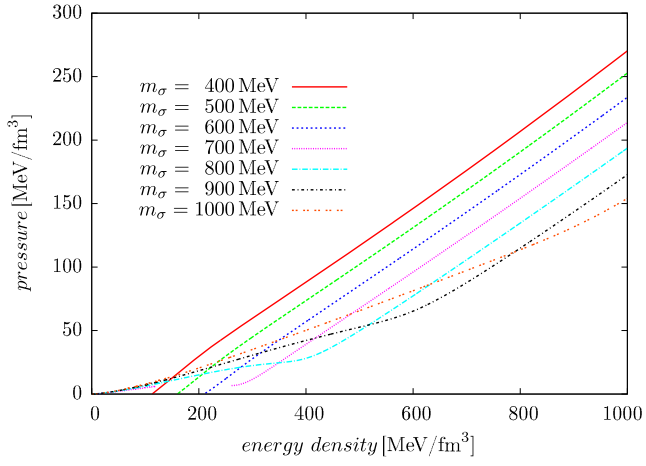

FIG. 8 (color online). $SU(3)$ quark-meson matter equation of state for $Y_e = 0.2$, $s = 1.0k_B$/baryon, $g_\omega = 3.0$ and different σ meson masses m_σ. At large energy densities the EoS shows the same slope and the curves are just shifted to higher energy densities with increasing values of m_σ. If the phase transition from the vacuum to the matter phase is a crossover, the lines have a smaller slope at small energy densities.

This high-density limit originates from the inclusion of the vector meson exchange, otherwise the limit would be $p = \epsilon/3$. Hence, a nonzero vector coupling results in the wrong high-density limit as dictated by asymptotic freedom of QCD; see [12,33] and the discussion in [34]. But at the energy densities that are considered here the impact of the contribution from the vector mesons are not strong enough to enter this regime. For the cases of a first-order phase transition from the vacuum to the matter phase an almost vanishing pressure for a nonvanishing energy density is found followed by a linear increase in the pressure. This behavior is not observed if the phase transition is a crossover as found for the largest considered vector couplings, since there is no jump in the energy density.

The influence of the σ mass on the quark-meson matter equation of state is shown in Fig. 8. One notices that the impact of varying the sigma meson mass is different for the low- and high-energy density regions. The slope of the curves are unaffected and the EoS is just shifted parallel in the high-energy density limit when varying m_σ. For a more massive scalar meson, the EoS has a lower pressure at the same energy density. However, differences occur at low-energy densities. If the phase transition from the vacuum to the matter phase is a crossover, i.e. for high σ meson masses, the slope of the EoS is much smaller compared to the high-energy density limit. Here, the EoS for higher values of m_σ has a higher pressure at the same energy density, contrary to the high-energy density limit.

V. SUMMARY

In this work the structure of the phase diagram and the high-density QCD plasma EoS calculated from the linear

sigma model in a mean field approximation were analyzed. The model was expanded by adding vector mesons, which give an additional contribution to the quark chemical potentials. Calculations for the two and three flavor cases were presented.

The parameters were fixed by measured meson masses and decay constants. The remaining free parameter, like the mass of the σ meson m_σ and the vector coupling constant g_ω, were varied and their influences on the phase diagram and the equation of state were investigated. The conditions characteristic for core-collapse supernova explosions served as further input. These are charge neutrality, β equilibrium with respect to weak interactions, and a given electron-baryon fraction.

The phase diagram was analyzed and a first-order phase transition from the vacuum to the matter phase at low temperatures was observed for certain parameters. For higher temperatures the phase transition line ends in a critical endpoint, after which the phase transition is a crossover. By increasing the vector meson coupling constant the phase transition gets shifted to higher μ_Q, but for too large values the first-order phase transition vanishes and a crossover is observed for all temperatures. The same behavior was seen for increasing σ masses. The effect of a lowered σ mass could be compensated by an increased value of g_ω.

The quark-meson matter equation of state was calculated for a given entropy per baryon, with typical values found in supernova simulations. The particular value for the entropy per baryon has little influences on the EoS. An increasing vector repulsion, i.e. increasing g_ω, leads to a higher slope of the EoS. Higher values of m_σ shift the EoS to lower pressures at constant energy densities. However, the slope of the EoS at high pressures stays constant, whereas at low-energy densities differences occur due to the change of the order of the phase transition.

Whether the computed equation of state is useful in a supernova explosion has to be tested in simulations. We stress that the model presented here lacks a low-density hadronic phase. Thus it should be matched at low-energy densities to a hadronic EoS for most cases, unless strange quark matter is absolutely stable at vanishing temperature. Instead of adding a low-density hadronic EoS to the quark-meson model the latter also has the potential to be extended to include baryonic degrees of freedom, leading to one single equation of state valid over the hole density range. For work in this direction by including diquarks in two-color QCD, see e.g. [35,36].

Recent improvements of the Polyakov-loop extension of the quark-meson model [21,37,38] can be considered in the presented framework and the conditions of supernova matter studied here can be worked into the investigation of the nucleation time scales of a quark phase [39,40].

More importantly, the quark meson model has to be confronted with the observed new mass limit for compact stars from the mass measurement of the pulsars PSR J1614-2230 with a mass of $M = 1.97 \pm 0.04 M_\odot$ [41] and PSR J0348 + 0432 [42] with a mass of $M = 2.01 \pm 0.04 M_\odot$. This is work in progress and will allow studies to constrain the parameter space more strictly than it was possible in this analysis [43].

ACKNOWLEDGMENTS

This work is supported by the German Federal Ministry of Education and Research (BMBF) under Grants No. FKZ 05P12VHCTG and No. 06HD7142, by the German Research Foundation (DFG) within the framework of the excellence initiative through the Heidelberg Graduate School of Fundamental Physics (HGSFP) and through the Helmholtz Graduate School for Heavy-Ion Research (HGS-HIRe) and the Graduate Program for Hadron and Ion Research (GP-HIR) by the Gesellschaft für Schwerionenforschung (GSI), Darmstadt and the Alliance Program of the Helmholtz Association HA216/EMMI.

[1] H.-T. Janka, Annu. Rev. Nucl. Part. Sci. **62**, 407 (2012).
[2] B. Kampfer, Astrophys. Space Sci. **93**, 185 (1983).
[3] M. Takahara and K. Sato, Phys. Lett. **156B**, 17 (1985).
[4] M. Takahara and K. Sato, Astrophys. J. **335**, 301 (1988).
[5] J. A. Pons, A. W. Steiner, M. Prakash, and J. M. Lattimer, Phys. Rev. Lett. **86**, 5223 (2001).
[6] I. Sagert, T. Fischer, M. Hempel, G. Pagliara, J. Schaffner-Bielich, A. Mezzacappa, F.-K. Thielemann, and M. Liebendörfer, Phys. Rev. Lett. **102**, 081101 (2009).
[7] T. Fischer, I. Sagert, M. Hempel, G. Pagliara, J. Schaffner-Bielich, and M. Liebendörfer, Classical Quantum Gravity **27**, 114102 (2010).
[8] B. Dasgupta, T. Fischer, S. Horiuchi, M. Liebendorfer, A. Mirizzi, I. Sagert, and J. Schaffner-Bielich, Phys. Rev. D **81**, 103005 (2010).
[9] A. Ohnishi, H. Ueda, T. Nakano, M. Ruggieri, and K. Sumiyoshi, Phys. Lett. B **704**, 284 (2011).
[10] A. Bauswein, H.-T. Janka, R. Oechslin, G. Pagliara, I. Sagert, J. Schaffner-Bielich, M. Hohle, and R. Neuhäuser, Phys. Rev. Lett. **103**, 011101 (2009).
[11] A. Bauswein, R. Oechslin, and H.-T. Janka, Phys. Rev. D **81**, 024012 (2010).
[12] E. S. Fraga, A. Kurkela, and A. Vuorinen, Astrophys. J. Lett. **781**, L25 (2014).

[13] A. W. Steiner, S. Reddy, and M. Prakash, Phys. Rev. D **66**, 094007 (2002).
[14] S. B. Ruester, V. Werth, M. Buballa, I. A. Shovkovy, and D. H. Rischke, Phys. Rev. D **73**, 034025 (2006).
[15] V. Laporta and M. Ruggieri, Phys. Lett. B **633**, 734 (2006).
[16] F. Sandin and D. Blaschke, Phys. Rev. D **75**, 125013 (2007).
[17] T. Fischer, D. Blaschke, M. Hempel, T. Klahn, R. Lastowiecki *et al.*, Phys. At. Nucl. **75**, 613 (2012).
[18] M. Gell-Mann and M. Levy, Nuovo Cimento **16**, 705 (1960).
[19] B.-J. Schaefer and M. Wagner, Phys. Rev. D **79**, 014018 (2009).
[20] J. T. Lenaghan, D. H. Rischke, and J. Schaffner-Bielich, Phys. Rev. D **62**, 085008 (2000).
[21] R. Stiele, E. S. Fraga, and J. Schaffner-Bielich, Phys. Lett. B **729**, 72 (2014).
[22] L. Ferroni and V. Koch, Phys. Rev. C **83**, 045205 (2011).
[23] J. Beringer *et al.* (Particle Data Group), Phys. Rev. D **86**, 010001 (2012).
[24] T. Fischer, I. Sagert, G. Pagliara, M. Hempel, J. Schaffner-Bielich, T. Rauscher, F.-K. Thielemann, R. Käppeli, G. Martínez-Pinedo, and M. Liebendörfer, Astrophys. J. Suppl. Ser. **194**, 39 (2011).
[25] D. Parganlija, P. Kovacs, G. Wolf, F. Giacosa, and D. H. Rischke, Phys. Rev. D **87**, 014011 (2013).
[26] C. Sasaki, B. Friman, and K. Redlich, Phys. Rev. D **75**, 054026 (2007).
[27] K. Fukushima, Phys. Rev. D **77**, 114028 (2008).
[28] A. Schmitt, Lect. Notes Phys. **811**, 1 (2010).
[29] J. Boguta and H. Stoecker, Phys. Lett. **120B**, 289 (1983).
[30] B. Waldhauser, J. Maruhn, H. Stoecker, and W. Greiner, Phys. Rev. C **38**, 1003 (1988).
[31] M. Buballa, Nucl. Phys. **A611**, 393 (1996).
[32] C. Lenzi and G. Lugones, Astrophys. J. **759**, 57 (2012).
[33] A. Kurkela, E. S. Fraga, J. Schaffner-Bielich, and A. Vuorinen, Astrophys. J. **789**, 127 (2014).
[34] M. Buballa, V. Dexheimer, A. Drago, E. Fraga, P. Haensel *et al.*, arXiv:1402.6911.
[35] N. Strodthoff, B.-J. Schaefer, and L. von Smekal, Phys. Rev. D **85**, 074007 (2012).
[36] N. Strodthoff and L. von Smekal, Phys. Lett. B **731**, 350 (2014).
[37] L. M. Haas, R. Stiele, J. Braun, J. M. Pawlowski, and J. Schaffner-Bielich, Phys. Rev. D **87**, 076004 (2013).
[38] T. K. Herbst, M. Mitter, J. M. Pawlowski, B.-J. Schaefer, and R. Stiele, Phys. Lett. B **731**, 248 (2014).
[39] B. Mintz, E. Fraga, G. Pagliara, and J. Schaffner-Bielich, Phys. Rev. D **81**, 123012 (2010).
[40] B. W. Mintz, R. Stiele, R. O. Ramos, and J. Schaffner-Bielich, Phys. Rev. D **87**, 036004 (2013).
[41] P. Demorest, T. Pennucci, S. Ransom, M. Roberts, and J. Hessels, Nature (London) **467**, 1081 (2010).
[42] J. Antoniadis, P. C. Freire, N. Wex, T. M. Tauris, R. S. Lynch *et al.*, Science **340**, 1233232 (2013).
[43] A. Zacchi, R. Stiele, and J. Schaffner-Bielich (work in progress)